JOURNAL OF MATERIALS SCIENCE 25 (1990) 2312–2320

Studies of ceramic–liquid metal reaction interfaces

J. A. YEOMANS*, T. F. PAGE‡
Department of Materials Science and Metallurgy, University of Cambridge, Pembroke Street, Cambridge CB2 3QZ, UK

An investigation has been made of the nature and extent of chemical reactions between various liquid metals and a range of engineering-grade ceramics typically used as cutting tool inserts. Such possible reactions are relevant to chemical wear effects during metal cutting but also relate to liquid metal containment by ceramics and ceramic–metal joining. The experimental procedure has involved immersing pre-polished ceramic sections in liquid metals for controlled times with subsequent sectioning and examination of the reaction interface. The ceramics studied were two alumina-based materials and five silicon nitrides and sialons. The metals were pure iron, pure nickel and four iron–nickel alloys (a mild steel, a stainless steel and two nickel-based superalloys) and span a range of Fe–Ni compositions. The reaction rates of the alumina materials were found to be much lower than those of the silicon nitride-based materials and reflect the chemical stability of the Al–O bond array. Zirconia-toughened alumina showed little evidence of reaction with clean iron alloys but substantial attack by oxygen-containing iron-based materials was found resulting in the formation of iron-aluminium spinel reaction products. Al_2O_3–TiC/N exhibited preferential metal attack of the carbonitride phase with dissolution and/or replacement of the TiC/N dispersion. Within the silicon nitride-based group, ferrous alloys were found to be more damaging than mainly nickel alloys and silicon nitrides were more readily attacked than sialons. The difference in behaviour between the sialons and silicon nitrides is attributed to alumina additions in the former group of materials increasing resistance to attack by molten metals. A detailed mechanism of attack for these mixed-phase ceramics is proposed whereby a silicon concentration gradient is established from the crystalline ceramic phases, through the glassy binding phase, to the metal. The result is dissolution of the crystalline phase and an increase in volume fraction of the glassy binder at the metal–ceramic interface with concomitant progressive disruption of the ceramic microstructure.

1. Introduction

The chemical stability of engineering-quality ceramics exposed to liquid metals is an important consideration in many applications. Examples include the containment of molten metals, the formation of ceramic–metal and brazed ceramic–ceramic joints and high speed metal cutting with ceramic tool tips. It is this third case which is directly relevant to the specific ceramic–metal couples considered here, but the underlying philosophies and experimental methods are universally applicable.

The amount of openly available experimental data pertaining to engineering ceramics subjected to liquid metal corrosion is small (e.g. [1]). Indeed, the erroneous belief that ceramics are intrinsically chemically inert to most environments has somewhat hindered the need for progress in this area. The chemical stability of tool material–workpiece couples has been addressed from a theoretical standpoint by Kramer and Suh [2] and Dearnley [3]. Although this approach has been able to rank pairs of materials in order of expected reactivity there are two major disadvantages. First, only thermodynamic and not kinetic factors are taken into account and secondly only one phase on each side of the couple is looked at (though more sophisticated methods could be devised). Thus, there is a need for more experimental data, especially when current experience shows that the thermochemical data needed for such calculations are unreliable (e.g. [4, 5]).

Experimentally, previous workers have studied the interaction of liquid metals with ceramics by using the sessile drop method (e.g. [6]), by totally immersing the ceramic in molten metal (e.g. [7]) or performing joining experiments which are very application-specific. In the sessile drop experiment, the contact angle between a metal droplet and the ceramic substrate is taken as a first indication of the degree of reaction. Subsequent cooling and sectioning allows the nature of the reaction

**Present address:* Department of Materials Science and Engineering, University of Surrey, Guildford, Surrey GU2 5XH, UK.
‡Materials Division, Department of Mechanical, Materials and Manufacturing Engineering, The University, Newcastle upon Tyne NE1 7RU, UK.

0022–2461/90 $03.00 + .12

TABLE I Microstructural characterization of the ceramics

Material	Approx. starting composition (in wt %)	Crystalline phases	Grain boundary composition‡
Al_2O_3-ZrO_2	4% ZrO_2–96% Al_2O_3	ZrO_2 particles in Al_2O_3	
Al_2O_3-TiC/N	30% TiC/N–70% Al_2O_3	TiC/N grains or clusters in Al_2O_3 matrix	
α'/β'-sialon (Starck)*	81% Si_3N_4, 6% Y_2O_3, 4% Al_2O_3, 10% AlN	α' and β' sialon (12H polytype and B phase in grain boundary region) in a glassy binding phase	40–55% Si, ~15% Al, 25–45% Y
α'/β'-sialon (Kema Nord)*			
β'-sialon	86% Si_3N_4 6% Y_2O_3 8% Al_2O_3	β'-sialon in a glassy binding phase	
SL100 (Feldmühle)†	90% Si_3N_4, 7% Y_2O_3, 3% Al_2O_3, SiO_2, FeO	Si_3N_4 (melilite and apatite in grain boundary region) in a glassy binding phase	~40% Si, ~60% Y
Iscanite (Iscar)†			

*The two α'/β'-sialons were made from different sources of Si_3N_4 powder. The Kema Nord variant produced a finer grain size material.
†These materials were the only two ceramics not supplied by Sandvik Hard Materials.
‡Approximate composition determined by EDS in TEM. Elements with Z < 11 not detected i.e. O and N.

to be examined. When the total immersion method is used the specimen is removed at the end of the test and the mass change recorded to allow a reaction rate to be evaluated. To do this, the ceramic–metal interface is usually destroyed and hence valuable information is lost.

In the present study, pre-polished, ceramic sections have been partially immersed in molten metal to allow a large area to react (which is not the case in sessile drop experiments) and the couple has then been allowed to cool as a single unit to preserve the interface for subsequent microstructural evaluation. Such examination of the reaction interface is vital if the mechanism of attack is to be understood. In turn this can lead to the selective refinements of the microstructure of a particular ceramic to produce a material more resistant to specific chemical attack.

2. Materials

The ceramic–metal couples investigated during this study were chosen to be of direct relevance to the metal cutting industry. All ceramics used were either commercially available cutting tools or experimental grades under evaluation as potential tool materials. The materials comprised a zirconia-toughened alumina (ZTA) containing ~4 wt % ZrO_2, an alumina-titanium carbonitride containing ~30% TiC/N, three sialons and two pressureless sintered silicon nitrides. A fuller description is given in Table I which also describes the microstructural constituents of each material. Micrographs of many of these microstructures have been published in a preliminary report [8] and almost all can be seen on the unreacted ceramic areas of Figs 2 to 9.

The metallic halves of the couples were mainly commercial alloys supplied in bar stock form. The materials span a range of Fe : Ni ratios from steels through to nickel-based alloys with substantial amounts of other elements present in some cases (notably chromium). These materials are representative of the most commonly encountered workpiece materials. Their nominal compositions are given in Table II. To complete the series, pure (99.99%) iron and nickel were also included. In one case a nominally pure iron powder was also used (see Section 4.1).

3. Experimental procedure

The ceramics were supplied by Sandvik Hard Materials as indexable tool inserts, as used for metal cutting. These have dimensions typically of 6 × 12 × 12 mm. Slices approximately 1 mm thick were cut from the inserts, perpendicular to the large faces, using a Capco Q35 high speed annular diamond saw. The two resultant large faces of the slices were ground and polished, using a series of diamond loaded laps and cloths, down to a 1 μm diamond finish. They were

TABLE II Manufacturers' analysis of the alloys

	C	Si	Cu	Fe	Mn	Cr	Ti	Co	Ni	S	Al Mo	P	Others
En8	0.42	0.29	–	bal	0.82	0.04	–	–	0.05	0.03	0.035 0.01	0.021	0.0030
En58J	0.043	0.48	0.34	bal	1.60	17.0	0.011	–	10.60	0.008	– 2.0	0.035	0.01Nb
Incoloy 901	0.034	0.16	0.09	bal	0.14	13.08	2.98	0.19	41.62	0.003	0.24 5.64	0.012	–
Inconel 718	0.052	0.14	0.08	bal	0.11	18.85	1.00	0.03	53.09	0.002	0.54 3.18	0.009	–

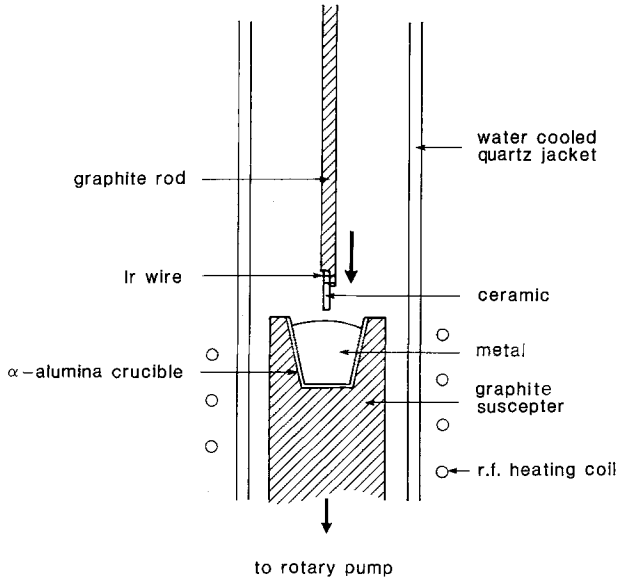

Figure 1 A schematic representation of the apparatus used to partly immerse ceramic sections in liquid metals and thus produce ceramic–metal reaction interfaces.

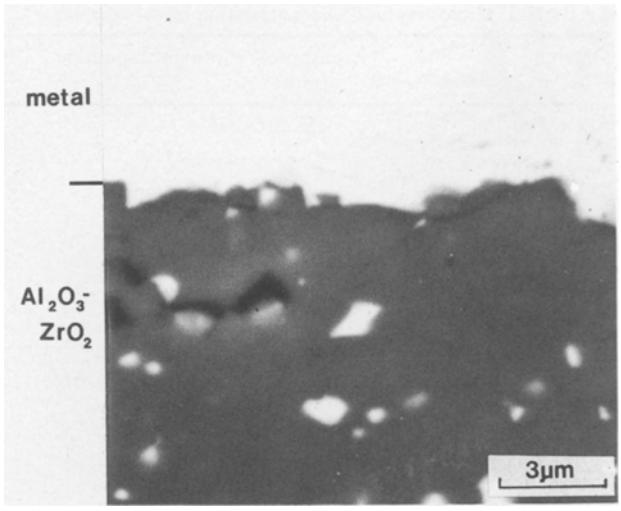

Figure 2 The interface formed between zirconia–toughened alumina and En8. The metal has wetted the ceramic but no discernible reaction has taken place. This is typical of all the ZTA–metal couples when the metal is from bar stock. (BSI/SEM 15 kV; the light-imaging features in the dark imaging alumina are ZrO_2 particles).

thoroughly ultrasonically cleaned in methanol prior to immersion testing.

The apparatus used for performing the immersion tests is shown in Fig. 1. A piece of ceramic was suspended over the crucible while the metal was heated to just above its melting point. Iridium wire was chosen to attach the ceramic to the support rod since iridium is unreactive with all the metals used (at least at their melting points). Once a pool of molten metal had been formed the ceramic, but not the graphite rod, was pushed into the metal allowing a reaction to take place. After 120 sec the power to the R F generator was cut off and the system allowed to cool to room temperature. All operations were performed in a stream of pure argon.

The experimental conditions were chosen to represent those possibly encountered at the metal–ceramic interface in metal cutting. Indeed, the metal chip that flows over the rake face of the ceramic tool tip is thought to resemble a liquid more than a solid [9]. In practice it is not quite molten so, at first sight, our experiments appear to have been conducted at higher temperatures than those encountered when machining. However, when machining, the chip is constantly flowing over the ceramic sweeping away any reaction products and thus enhancing the reaction rate. By contrast the higher reaction rates created by the higher temperatures in the immersion test are partly countered by the static interfacial region where the lack of flow would be expected to lead to lower reaction rates. In practice, these effects are at least partly self-compensating. The time of immersion was chosen to be 120 sec as this is a typical contact time for a ceramic tool tip machining these types of workpiece. The argon was needed to exclude a reactive environment, such as air, from the interface, again to reproduce the metal cutting situation. The validity of this approach is supported by the good correlation of behaviour in this test with observed wear rates of ceramic tool tips [8, 10]. After the R F power was cut-off, solidification of the molten pool was almost instantaneous with subsequent cool down taking about 60 min. Since reaction rates with liquid metals are expected to be much faster than with solid metals even at the same temperature, the molten period is thought to dominate the resultant observations in all cases.

On reaching room temperature the ceramic–metal couple was removed from the apparatus and sectioned parallel to the top metal surface and roughly in the centre of the immersed length of ceramic. Previous multiple sectioning of specimens had shown the reaction front to be reasonably even along the length of the ceramic making the exact position of the section unimportant. The two halves of the couple were then mounted cut sides up in bakelite and polished using conventional metallographic techniques. The surface finish over the entire specimen was never very good because of the difference in hardness between the metal and the ceramic, but was adequate to distinguish the features in the interfacial zone which was of most interest.

Polished samples were then coated with a thin layer of carbon to render the surfaces electrically conductive and viewed in a variety of scanning electron microscopes (SEMs). Backscattered and secondary electron imaging was performed using a CamScan S4. Energy dispersive X-ray spectroscopy (EDS) was performed using an ISI 100A and a CamScan S4 (courtesy of CamScan at their Bar Hill premises). Both microscopes were fitted with a Link Systems conventional beryllium-window EDS detector and spectra were analysed using an AN 10000 processor. Four specimens were also analysed with electron probe microanalysis (EPMA) using a Camebax microprobe (courtesy of M. Mikus, Sandvik Hard Materials, Stockholm). All micrographs in this paper are taken in backscattered electron image (BSI) mode, to reveal atomic number contrast.

4. Results and discussion

Since there are seven ceramics interacting with six

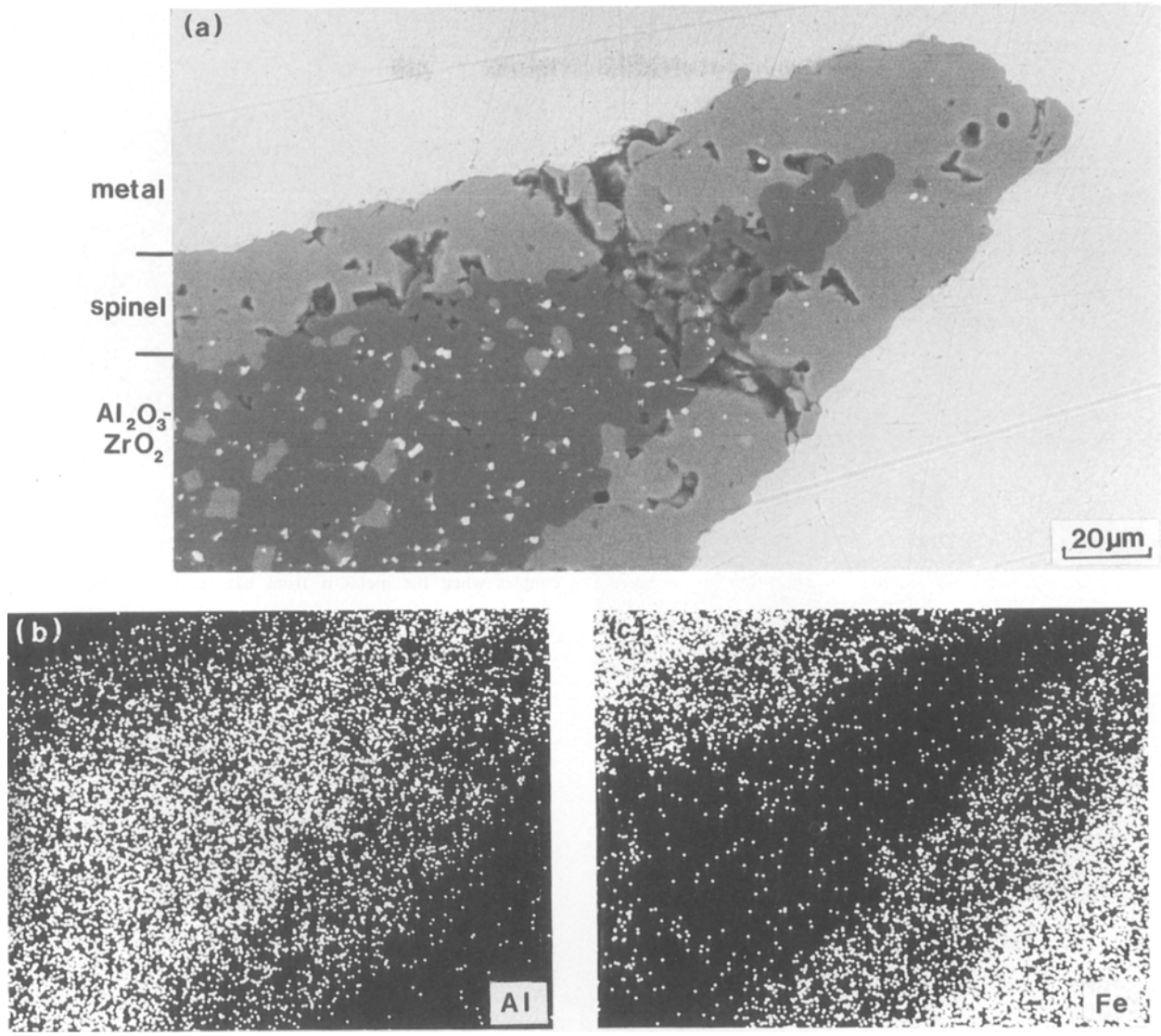

Figure 3 (a) The substantial interfacial reaction product (spinel) formed between the metal and ceramic when zirconia-toughened alumina reacted with iron from a powder source (and presumed to contain iron oxides). (b), (c) EDS X-ray dot maps for aluminium and iron; the presence of oxygen has been inferred.

metals, 42 reaction couples were studied. However, since a number of principles emerge from the studies, each couple need not be dealt with individually. Minor differences will be ignored here though a full description is available elsewhere [10]. Rather, the results will be presented grouped by ceramics, since it is the development of wear scars and reaction structures on particular materials, together with the behavioural trends of individual ceramic systems which are usually of the greater concern when considering ceramic–liquid metal interactions.

4.1. Zirconia-toughened alumina (ZTA)

The ZTA specimens showed no detectable interaction with any of the metals from bar stock sources. As shown in Fig. 2, the metals wetted the ZTA and penetrated surface irregularities. Since the depth of penetration is of the same order of magnitude as the grain size, it is not clear whether the metal flowed into sites of grain pull-out from the polishing process or whether very mild, localized attack occurred. The zirconia particles within the ceramic were unaffected, as would be expected from theoretical considerations (from [2] the relative solubilities of ZrO_2 and Al_2O_3 in α-iron at 1600 K are 3.8×10^{-8} mol % and 5.55×10^{-7} mol % respectively). A typical interface is shown in Fig. 2.

ZTA was also immersed in a melt derived from an iron powder. In this case a $\sim 15\,\mu$m thick reaction zone was formed inwards from the original surface of the ceramic towards the ceramic interior (see Fig. 3a). Both aluminium and iron were detected by EDS within the zone (Figs 3b and 3c). It is also likely that a small amount of zirconium is present in the solid solution since the zirconia particles are less apparent in the region of the zone closest to the metal, suggesting that they have dissolved in the reaction product after its formation. No iron was detected in the ceramic past the reaction zone and no aluminium was detected in the metal. The image grey level of this reaction product is slightly higher than that of the ZTA and it is assumed to be some form of spinel. The difference of behaviour between the iron from the two sources is attributed to the difference in oxygen content. Each iron particle will be surrounded by a layer of oxide, thus the oxide content will be much greater for the

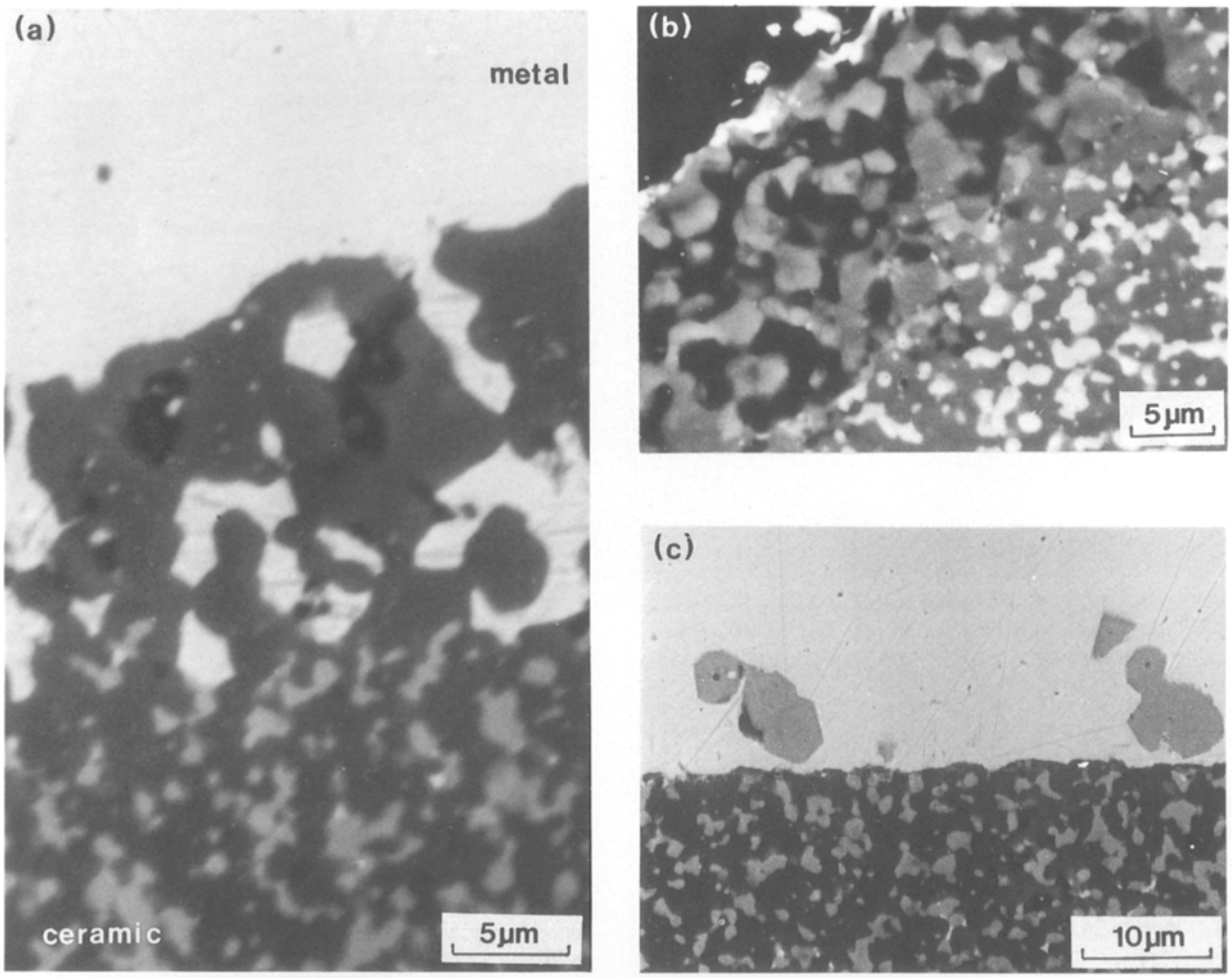

Figure 4 (a) Replacement of titanium carbonitride (lighter imaging phase in the Al_2O_3 on the lower part of the micrograph) with En58J. Coarsening of the alumina grain structure within the first 15 to 20 μm of the interface is also evident. Note the similar grey levels displayed by the En58J and the material replacing the TiC/N in the upper part of the ceramic. (b) Removal of TiC/N by nickel with no metal replacement. (c) An example of large crystals of a titanium compound appearing in the metal near the metal–ceramic interface. The BSI grey level is the same as for the TiC/N in the ceramic.

powder than the large pieces of iron from bar stock. As expected from phase equilibria data [11], the alumina appears to have been attacked by the oxide to form a mixed spinel whereas it would seem to be inert to the iron. This also confirms that the argon flowing through the apparatus during the experiments is preventing substantial oxidation of the molten metals from bar stock. This is important if the results are to be relevant to metal cutting, since the environment is thought to be excluded from the chip–tool interface during machining, though it may be able to have more ready access at the edge of the moving chip, i.e. around the depth-of-cut ("notch") wear scar.

4.2. Alumina–titanium carbonitride

Reactions between the alumina–titanium carbonitride and the various metals were limited to the outside 15 to 20 μm of the ceramic. The general trend was for the TiC/N particles to be replaced by the metal and the microstructure within the layer to be much coarser, i.e. the alumina was also affected. Typical sections of interfaces are shown in Fig. 4. Fig. 4a shows the case in which the TiC/N array is replaced by a ferrous alloy (En58J). The titanium, carbon and nitrogen would be expected to reside in the metal in solution, though this was not confirmed experimentally. However, there were two exceptions to this general behaviour.

In the case of the nickel, a reaction zone was formed in which the TiC/N had been lost from the first 15 to 20 μm but had not always been replaced by nickel so a porous alumina structure was left (Fig. 4b).

With Incoloy 901, no obvious reaction zone was found though large particles of a titanium compound were observed within micrometres of the ceramic surface (Fig. 4c). These were tentatively identified as reprecipitated TiC/N, since they showed the same grey level in the BSI–SEM image as TiC/N.

It would seem that, in all the alumina–titanium carbonitride experiments there is a tendency for the titanium carbonitride to be preferentially attacked and removed from the alumina matrix. If it is replaced by a metal there may be some further internal reaction with the alumina. The reactions are not particularly severe with ceramic being consumed at the rate of about 10 μm per min. Indeed this type of behaviour may well be beneficial when attempting to join alumina–titanium carbonitride to a metal. However, the mechanism of attack is unclear. The TiC/N dispersion is not connected together in the way that these observations might suggest. Thus, the most likely diffusion path by which the metallic phase

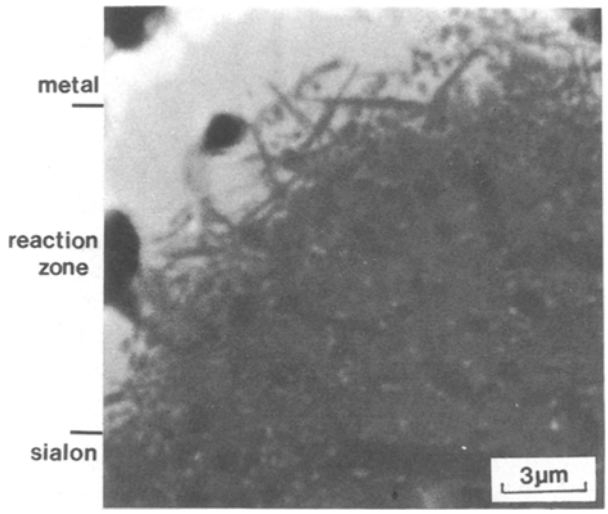

Figure 5 A typical sialon–metal interface revealing metal (white), an aggregation of matrix binding phase from the sialon and a region over which the true sialon microstructure is left unaffected. Sialon grains can be seen to be dissolving in the surface film of matrix binding phase with a resultant "loosening" of the structure (and enrichment of the silicate binding phase). The matrix binding phase–metal interface is approximately 20 μm from the virgin ceramic as shown.

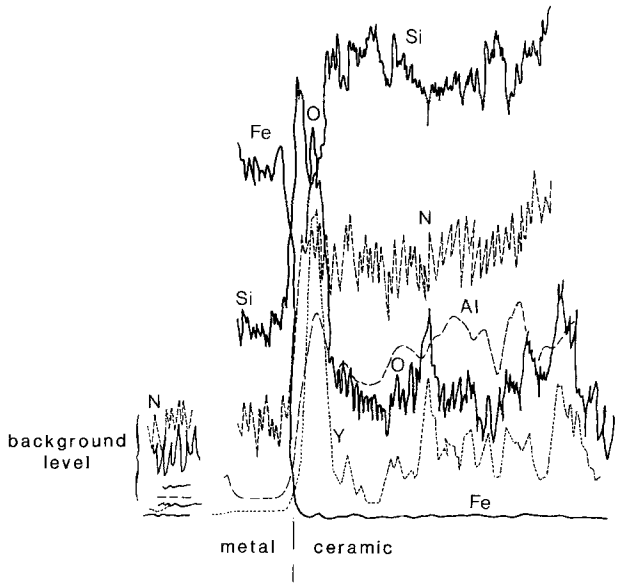

Figure 6 Microprobe line scans across the Starck α'/β'-sialon–iron interface. It is clear that silicon, but no other elements, are present in the iron; aluminium, oxygen and yttrium concentrations all peak at the edge of the ceramic corresponding to the presence of the enriched matrix binding phase. The nitrogen level is fairly constant across the ceramic then drops to zero at the interface; nitrogen is presumed to be lost from the system as a gas.

penetrates to the TiC/N dispersion is around the grain boundaries of the alumina matrix and this might further explain the grain growth exhibited by the alumina. In this case, the alumina does not remain unaffected and that may have important consequences for the behaviour of other alumina mixed-phase ceramics and ceramic matrix composites. For example Al_2O_3–SiC_w (whiskers) composites are known to be readily attacked by ferrous alloys with replacement of the SiC_w distribution by metal [12]. However, in this case the whisker array is known (by etching away the matrix) to be fairly well-connected spatially [12] and thus differs from the TiC/N dispersion here. In the Al_2O_3–SiC_w case, no grain growth of the alumina accompanies the chemical attack [12].

4.3. The sialons

The three sialons showed broadly similar behaviour. When differences did occur this was due to the Kema Nord variant showing a more rapid reaction than the other two sialons. The reaction zones formed by the two α'/β'-sialons interacting with pure iron and pure nickel were studied using a microprobe, so most information is known about these four samples. These results will be used as the basis for discussion of the sialon results and differences in behaviour will be noted afterwards.

A typical sialon–metal interface is shown in Fig. 5. Towards the interface, the sialon structure appears "looser" than normal and further, there is a substantial layer of material on the ceramic side of the reaction interface. The grey level and composition suggest that it is the silicate binder from the sialon. This enhanced proportion of matrix binding phase suggests that some of the crystalline grains have dissolved and their constituent elements (Si, Al, Y, O and N) have either entered the surrounding glass or left the ceramic system to go into the metal. Microprobe line scans across the interface show higher concentrations of aluminium, yttrium and oxygen within the film of binding phase (Fig. 6). The silicon level peaks when a sialon grain is traversed and continues into the metal (whether iron or nickel). The nitrogen level is fairly even across the ceramic side of the interface then drops to zero when the metal is reached, suggesting that it is being lost from the system, presumably as a gas. Sometimes such gas bubbles are seen in the

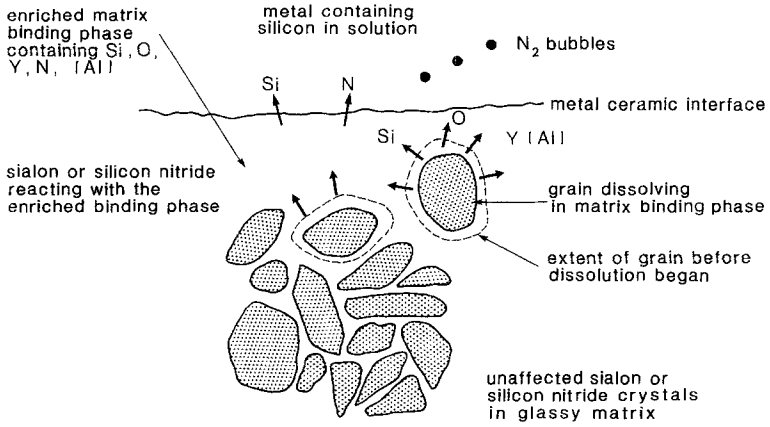

Figure 7 A schematic illustration of the proposed mechanism of reaction between sialons/silicon nitrides and liquid metals. There will be an activity gradient for silicon towards the metal interface.

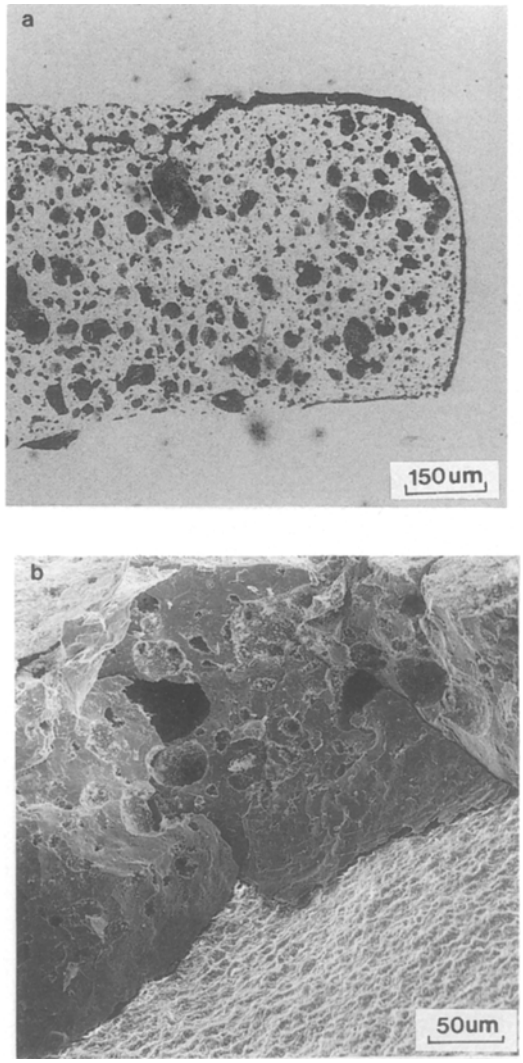

Figure 8 (a) Total consumption of the SL100 silicon nitride after immersion in molten En58J. The ceramic has been replaced by a porous metal containing islands of the original matrix binding phase together with bubbles presumed to be nitrogen from the decomposition of Si_3N_4. (b) A SEM micrograph of a region from the metal–ceramic interface of the Iscanite Si_3N_4/En58J couple, again showing the highly porous nature of the metal still adherent to the ceramic surface.

ceramic (Fig. 5) though more often they are observed in the metal (see later). No metal was detected in the ceramic and only silicon was detected in the metal. Thus, the mechanism of attack would appear to be transfer of silicon into the metal from either direct contact with the sialon grains or, as seems more likely from the microstructural evidence, via the matrix binding phase. As silicon is transferred from the binder to the metal, the now silicon-depleted glassy phase regains its silicon through dissolution of more sialon grains and thus essentially acts as a diffusion path for the silicon to enter the metal. Nitrogen released by the reduction of the sialon is mainly lost from the system as a gas (though some is likely to reside in the matrix silicate phase). The other elements released from the sialon grains (aluminium, oxygen, yttrium) appear to enter and remain in the binding phase presumably forming a glassy silicate structure. This is summarized and shown schematically in Fig. 7. The iron–silicon and nickel–silicon phase diagrams confirm the mutual solubility of the respective metal and silicon above the melting points of the metals. It is also known that the presence of silicon in iron decreases the solubility of both aluminium [13] and nitrogen [14].

The reaction of the Kema Nord variant with iron was more pronounced than the other three couples examined in detail. The ceramic was attacked to depths $\sim 200\,\mu m$ in places. The metal occupying the prior ceramic positions was porous, again suggesting that gas (nitrogen) evolution had taken place. The iron had taken silicon into solution but was also found to contain islands of a second phase. This phase has corresponding peaks in the aluminium, oxygen and yttrium microprobe traces. It may also contain nitrogen and silicon but due to the problems associated with possible penetration of the electron beam through the particles to the matrix beneath, it is not possible to be definite about the composition of the second phase. However, it seems to be very similar to the enriched matrix binding phase of the other specimens. When the rate of attack by the metal is more severe (see below) or the contact times are longer, the metal seems to be able to disrupt the now porous ceramic incorporating remnants of the silicate matrix into itself and sweeping past to consume more ceramic. Hence the Kema Nord–iron specimen represents an extension of the mechanism postulated in the preceding discussion.

Indeed, the mechanism of attack would appear to be the same for all the sialon–metal couples but the severity of attack is both sialon- and metal-dependent. In most cases, reaction zones are of the order of tens of micrometres, the superalloys and nickel tending to produce less disruption of the ceramic than the more ferrous alloys. This may be due to the large negative deviation from Raoult's Law shown by silicon in molten iron which would lead to steeper activity gradients than would be predicted [15]. The attack of Kema Nord by pure iron and En58J were the most severe cases of damage to the ceramic. Compositionally the Starck and Kema Nord variants are very similar. However, the Kema Nord has a finer grain size and this is the most likely explanation for the differences in the rate of degradation. If the mechanism of dissolution of sialon grains is correct then the material with the larger grain surface area would be expected to be the more readily attacked, as is observed.

4.4. The pressureless sintered silicon nitrides

The predominantly ferrous metals (pure iron, En8 and En58J) all react with the silicon nitrides to disrupt the ceramic microstructure. Reaction zones are 200 to $300\,\mu m$ deep and, in the case of a thin specimen of SL100 immersed in En58J, the entire ceramic was consumed (see Fig. 8a). In all these cases the ceramic in the reaction zone has been replaced by a porous (presumed nitrogen bubble) metal containing silicon in solution and a second phase containing silicon, yttrium and oxygen (the presence of oxygen is inferred since it was not detected by EDS). Aluminium is not present in this second phase since it does not occur in the silicon nitride in any appreciable quantity. The mechanism of attack is presumed to be the same as for

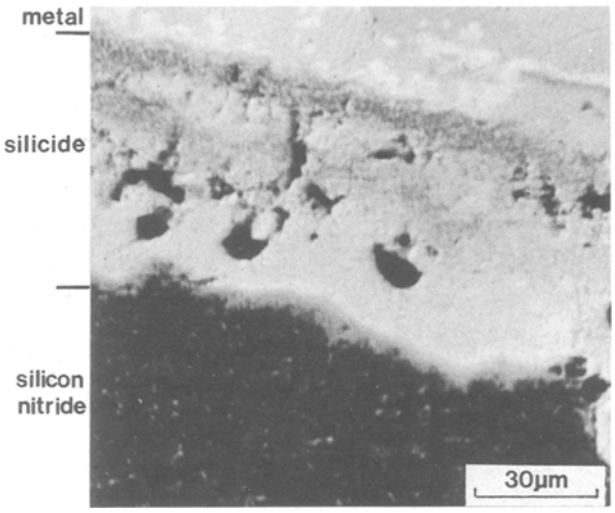

Figure 9 Typical reaction product, presumably a silicide, formed between dark imaging silicon nitride (SL 100) and nickel based superalloys (Inconel 718).

Kema Nord/En58J. Fig. 8b shows a micrograph from a fractured Iscanite/En58J interfacial zone in which the porous metallic phase is clearly visible.

The reactions with the nickel-based superalloys were not so severe. The ceramics were attacked to depths of a few tens of micrometres and a second phase was formed between the metal and the ceramic (Fig. 9). This was found to contain the metallic elements chromium, nickel and tantalum, (in the case of Inconel 718), as well as silicon. It seems likely that silicide formation has taken place. The formation of silicides (which also contain nitrogen) and their break down, under certain conditions, with the take up of either or both of silicon and nitrogen by the metallic phase, has been observed in the study of the solid state reactions between silicon nitride and several iron- and nickel-based alloys [16]. The reaction with nickel was as described for the sialons.

4.5. General discussion of the immersion test results

The first major division in the results is between the aluminas and the silicon nitride-based ceramics. Alumina appears to be unaffected by molten metals unless either another metal oxide is present (or forms) which is capable of dissolving alumina, or a second phase within the alumina matrix is attacked. Zirconia has been observed to be unaffected by the metals but titanium carbonitride is removed (and presumably decomposed and dissolved). The rates of reaction for the aluminas are the lowest observed in this series of experiments. The path by which the metals penetrate to the unconnected TiC/N disperion is presumed to be by the alumina grain boundaries which may be chemically different in this sample to those in ZTA. This same mechanism also seems to cause significant grain growth of the alumina.

Broadly, the sialons and silicon nitrides all undergo the same type of dissolution mechanism whereby silicon is taken into solution by the metal and the prior matrix binding phase becomes enriched by the elements not taken up by the metal and increases in volume, forming discrete islands in the metallic phase if attack is severe. However, the ceramics, especially the silicon nitrides, seem to be more prone to attack by predominantly ferrous metals. All other things being equal, a smaller grain size material also appears to be less resistant to the ingress of molten metals.

The effect of grain size is easy to understand in terms of greater surface area but the other differences in behaviour are less obvious. The major difference between the silicon nitrides and the sialons is the amount of alumina present in the initial compositions. Alumina becomes incorporated into the microstructure of a sialon in two ways. Aluminium and oxygen substitute for silicon and nitrogen in the original silicon nitride tetrahedra giving rise to sialon grains. Also alumina participates in the formation of the matrix binding phase. This is a liquid at the sintering temperature formed by the reaction of the silica, which is present on every silicon nitride grain, with the other oxides. The liquid solidifies on cooling to form a silicate glass, crystalline phases, or a mixture of the two, depending on the composition and the cooling rate [17]. For the materials considered in this study the majority of the matrix binding phase is a glass. Alumina is an intermediate glass former capable of forming a network with silica whereas yttria is a modifier which breaks up silicate structures. Thus, it appears that the addition chemical stability of the Al–O bond can be conferred on both the crystalline and glassy binding phases.

The work on ZTA has shown the Al–O bond array to be resistant to molten metal attack: thus sialon grains might be expected to dissolve more slowly than silicon nitride grains. This hypothesis is supported by the wear data of Aucote and Foster [18]. A series of sialons were used to machine Inconel 901. Flank wear was attributed to a chemical reaction with and dissolution in the workpiece. Wear resistance was found to increase with increasing α' content of the material and with increasing z values of the β' sialon grains (where z is defined by the substitution formula $Si_{6-z}Al_zO_zN_{8-z}$) indicating that more alumina leads to less wear by dissolution.

The nature of the grain boundary phase will also affect the rate of reaction. The sialon grains are surrounded by an alumina–silica–yttria glass whilst the silicon nitride grains are surrounded by a silica–yttria glass containing some crystalline phases. Due to the different network effects of alumina and yttria the sialon matrices would be expected to be more difficult to disrupt physically as well as being chemically more stable. Thus, the amount of alumina present in the silicon nitride-based materials is thought to be an important factor in controlling their resistance to molten metal attack.

5. Conclusions

The reactions of a series of ceramic–liquid metal couples relevant to the metal cutting industry have been investigated. Al–O bonds in alumina have been shown experimentally to be resistant to attack from iron and nickel and their alloys providing that the oxide content of the metal is low and that they are not

in close proximity to a more reactive phase such as titanium carbonitride.

Silicon nitride based materials show reaction rates which are metal dependent. Predominantly ferrous alloys cause more damage than nickel ones. Sialons are more resistant to attack than silicon nitrides. The mechanism of attack is thought to involve take up of silicon by the metal, leading to an activity gradient which itself causes dissolution of sialon/silicon nitride grains. Nitrogen is lost as a gas from the system and the other elements released by the break up of the grains enter the silicate matrix binding phase increasing its volume and changing its composition. In cases of severe disruption of the ceramic the silicate phase is incorporated as islands into the metallic phase which is also porous due to the gas evolution.

The difference in behaviour between the sialons and silicon nitrides is attributed to the presence of Al–O bonds in the former. These are thought to make the grains more resistant to dissolution and the matrix binding phase more chemically stable and physically more difficult to disrupt. Differences in behaviour between two grades of sialon of nominally the same composition suggest that finer grain size materials are more readily attacked due to the higher proportion of grain surface area.

Acknowledgements

The authors would like to thank Professor D. Hull F.R.S. F.Eng and formerly Professor R. W. K. Honeycombe F.R.S. F. Eng for the provision of laboratory facilities. JAY acknowledges financial support from SERC under the CASE scheme with Sandvik Hard Materials UK. Colleagues at Sandvik (in both Stockholm and Coventry UK) are thanked for their interest in and support of the project. Ms Gail Hepple kindly typed the manuscript.

References

1. D. B. BINNS, *Trans. J. Brit. Ceram. Soc.* **77** (1978) 1.
2. B. M. KRAMER and N. P. SUH, *J. Eng. Ind.* **102** (1980) 303.
3. P. A. DEARNLEY, *Surf. Eng.* **1** (1985) 43.
4. W. B. HILLIG, in "Tailoring Multiphase and Composite Ceramics" edited by R. E. Tressler *et al.* (Plenum Press, New York, 1986) p. 697.
5. A. WHITEHEAD and T. F. PAGE, *Ceram. Eng. Sci. Proc.* **10** (1989) 1108.
6. W. M. ARMSTRONG, A. C. D. CHAKLADER and J. F. CLARKE, *J. Amer. Ceram. Soc.* **45** (1962) 115.
7. K. H. JACK, *J. Mater. Sci.* **11** (1976) 1135.
8. J. A. YEOMANS and T. F. PAGE, *Wear* **131** (1989) 163.
9. E. M. TRENT, "Metal Cutting", 2nd edn, (Butterworths, Guildford, UK, 1984) p. 29.
10. J. A. YEOMANS, Ph.D. Thesis, University of Cambridge, (1986).
11. C. M. LEVIN, C. R. ROBBINS and H. F. McMURDIE, Phase Diagrams for Ceramists (American Ceramic Society, Ohio, USA, 1964).
12. R. BARRETT and T. F. PAGE, "Wear of Materials 1989" edited by K. C. Ludema (ASME, Ohio, USA, 1989) p. 441.
13. G. DERGE, "Basic Open Hearth Steelmaking", (AIMMPE, New York, 1964).
14. J. KUNZE, P. O. and K. FRIEDRICH, *J. Mater. Sci. Lett.* **5** (1986) 815.
15. A. E. PASTO, *J. Amer. Ceram. Soc.* **67** (1984) C178.
16. M. J. BENNETT and M. R. HOULTON, *J. Mater. Sci.* **14** (1979) 184.
17. M. H. LEWIS and R. J. LUMBY, *Powder Met.* **26** (1983) 73.
18. J. AUCOTE and S. R. FOSTER, *Mat. Sci. Technol.* **2** (1986) 700.

Received 13 April
and accepted 17 August 1989